Catalysis Today 174 (2011) 114–120

Contents lists available at ScienceDirect

Catalysis Today

journal homepage: www.elsevier.com/locate/cattod

Photocatalytic degradation of dye and NO_x using visible-light-responsive carbon-containing TiO_2

Yao-Hsuan Tseng*, Chien-Hung Kuo

Department of Chemical Engineering, National Taiwan University of Science and Technology, Taiwan

ARTICLE INFO

Article history:
Received 6 October 2010
Received in revised form 28 January 2011
Accepted 8 February 2011
Available online 12 March 2011

Keywords:
Carbon-containing TiO_2
Impregnation
Visible-light response
NO
Methyl orange

ABSTRACT

Ultraviolet- and visible-light-responsive titania was synthesized and employed in the photomineralization of NO_x and dyes. A carbon-modified titania photocatalyst was prepared by an impregnation method using anatase TiO_2 particles as the raw material and ethanol as the carbon source. Carbon-containing titanium dioxide with the anatase phase prepared at 200 °C, exhibited high photocatalytic activity for the degradation of gaseous NO_x and decolorization of aqueous methyl orange under visible-light illumination. The calcination temperature in this impregnation process plays an important role in the formation and resultant content of carbonaceous structure on TiO_2 surface and affects both the optical and the photocatalytic properties of TiO_2. The carbonaceous species on the TiO_2 surface, shown by photoluminescence spectroscopy, Raman, UV–vis, infrared spectroscopy, and X-ray photoelectron spectroscopes, plays an important role in the visible-light absorption and photocatalytic degradation rates for NO_x and methyl orange.

1. Introduction

Since the discovery of the photoelectrochemical splitting of water using titanium dioxide electrodes [1], researchers have extensively studied semiconductor-based photocatalysis. Currently, titanium dioxide is the most commonly used material for photocatalysts owing to its strong redox ability and widespread use in air purification systems, water treatment, deodorization, self-cleaning and sterilization coatings [1–3], and other applications. In environmental applications, TiO_2 exhibits excellent photocatalytic abilities for mineralizing NO_x, SO_x, and VOCs under solar irradiation; TiO_2 absorbs photons and evolves active oxygen species, such as OH radicals and O_2^- ions, through reaction with H_2O and O_2 adsorbed on its surface. The high oxidation potentials of these nascent active oxygen species result in the decomposition of many different pollutants [2,3].

A large number of photocatalytic applications use nano-sized anatase phase TiO_2. A light source of less than 388 nm in wavelength can activate a TiO_2 photocatalyst with an energy gap of 3.2 eV. In the solar light spectrum of the earth's surface, the energy associated with the UV region of wavelength from 280–400 nm accounts for only approximately 4% of the total energy. Meanwhile, the 400–700 nm wavelength visible-light region accounts for 45% of the total energy. Furthermore, UV light intensity, i.e., 0.1–5 $\mu W/cm^2$, is very low in indoor illumination situations limiting the domestic and indoor commercial applications for TiO_2. As a result, visible-light-responsive photocatalysts receive much more attention for increasing solar and indoor lighting energy utilization. Previous studies considered the sol–gel method, sputtering plasma, metal–organic chemical vapor deposition (CVD), physical vapor deposition (PVD), and metal ion-implantation methods to enhance the visible-light response of TiO_2. However, the equipment required for these methods is expensive, and mass production is difficult. Materials such as CdS, TaN, TaON, and $InVO_4$ are known to function as visible-light-responsive photocatalysts. However, in developing their widespread, large-scale use for any practical application, the cost and stability of the material must be considered. Few feasibility studies exist for these methods and materials for industrial-scale production owing to their higher cost, environment pollution issues, and material instability. In contrast, an impregnation process followed by low-temperature calcination is a practical way to produce visible-light-responsive TiO_2 materials because it enables the manufacturer to modify the commercial product effectively with only low operating costs.

Herein, we present a facile and cost-effective method for the preparation of high-efficiency visible-light-responsive TiO_2 developed using an impregnation method. The impregnation method is widely used to modify metal oxide particles and films. Normally, the impregnants used for the improvement of visible-light response in materials are noble metal salts, such as Pt, Au, and Ag [4–7]. The anions of N, S, C, P are inexpensive materials for the same purpose [2,3,8], but the processes used for their incorporation into the TiO_2

* Corresponding author. Tel.: +886 227 376 765; fax: +886 227 376 644.
E-mail address: tyh@mail.ntust.edu.tw (Y.-H. Tseng).

0920-5861/$ – see front matter © 2011 Elsevier B.V. All rights reserved.
doi:10.1016/j.cattod.2011.02.011

lattice as dopants are complicated and include the sol–gel method, sputtering plasma, metal–organic chemical vapor deposition, and ion implantation. Carbon-modified titanina is reported to exhibit good visible-light-responsive activity [4,9–21]. A carbon-modified photocatalyst has a great potential for practical application owing to the low cost of carbon sources. Vapor deposition methods (CVD and PVD) for the preparation of C-TiO_2 are quite effective [18–21], but rendered impracticable by expensive apparatus and complex processes. Therefore, wet-chemical [9–15] and mechanochemical [16] methods have been developed in order to reduce production costs. Visible-light-responsive C-TiO_2 can be synthesized by modified sol–gel processes using tetrabutyl orthotitanate as the precursor under controlled calcination conditions [9–15]. Kish et al. developed a commercial process for a carbon-modified photocatalyst prepared by the hydrolysis of titanium tetrachloride with tetrabutylammonium hydroxide [13–15]. However, these organic and inorganic precursors and related methods are also expensive and complicated, respectively. Thus, the most practicable approach for the mass production of visible-light-responsive TiO_2 is to directly modify the commercial UV-responsive TiO_2 material by a simple process. Herein we report the development of a simple impregnation process to prepare our carbon-containing photocatalyst using ethanol as the carbon source. The activities of the synthesized photocatalysts were evaluated for the oxidation of NO_x and decolorization of dye under illumination by visible light. The characteristics of these synthesized photocatalysts were also investigated for a satisfactory explanation of the visible-light activity.

2. Experimental

2.1. Experimental conditions and characterization

The carbon-containing, nano-structured TiO_2 samples were produced by the impregnation method. TiO_2 powder (10 g, Ishihara ST01) was added to anhydrous ethanol (100 mL) in a 250 mL flask. The solution was uniformly agitated at 500 rpm for 1 h, and then, the precipitated TiO_2 was obtained after drying at 70 °C on a hotplate. The dried powder was calcinated in air under controlled temperatures (100–300 °C) for 5 h. Sample nomenclature is defined as follows: TiO_2_X is the photocatalyst prepared by the impregnation process with calcination at X °C (100, 200, 250, and 300 °C) for 5 h.

The photocatalyst crystal phase was identified using X-ray diffraction with Cu Kα radiation (Rigaku D/Max RC). Material compositions and the content of carbonaceous species were determined by X-ray photoelectron spectroscopy (Perkin Elmer SSI-M probe XPS system). A diffuse-reflectance scanning spectrophotometer (Shimadzu, UV-2450) was employed to obtain the UV–vis absorption spectra of the powders. The reflectance data were converted to the absorbance values, $F(R)$, based on the Kubelka–Munk theory. Photoluminescence spectroscopy (PL) was carried out using a luminescence spectrometer (Jasco FP-6500LE), under excitation with 325 nm irradiation. The functional groups on the TiO_2 surface were observed with an infrared spectrometer (Thermo Nicolet Magna 750 II) equipped with a diffuse-reflectance device. Photoactalyst surface structures were identified by a Raman spectrometer (Renishaw 1000B), and a scattering experiment was conducted with a low-power green laser (30 mW) at 532 nm for 10 s.

2.2. Photocatalytic capacity of photocatalyst

2.2.1. Gaseous compound: degradation of NO

In this work, a continuous flow system is used for the degradation of NO_x over TiO_2 [4,9,10,19]. A cylindrical Pyrex glass vessel ($\phi \times H$, 10 cm × 4 cm) was used as the photoreactor for the degradation of NO_x, and a sample dish was located inside the vessel containing the TiO_2 powder. LEDs (visible light) or a black lamp (UV light) provided a light source with an intensity of 1 mW/cm^2. Two types of LED devices (blue and green) and one black lamp were used to provide visible light and UV light, respectively. The main LED and UV peaks are observed at 465, 515, and 352 nm, respectively. NO_x degradation was carried out at room temperature using an air stream containing 1.0 ppm NO as feedstock. Two mass flow controllers (MFCs) (Brooks 5850E) manipulated the relative humidity (RH = 50%) in the feeding stream. The reaction gas in the feeding stream passed through the vessel containing TiO_2 powder (0.2 g) at a flow rate of 1 L min^{-1}, with a residence time of 0.31 min. An on-line chemiluminescent NO_x analyzer (Eco Physics, CLD 700 AL) continuously monitored NO and NO_2 concentrations for gas analysis in the outlet.

2.2.2. Aquatic compound: decolorization of dye

Methyl orange ($C_{14}H_{14}N_3NaO_3S$) was used to investigate the photocatalytic activity of the TiO_2 samples under UV and visible-light illumination. 0.2 g of the photocatalyst was dispersed in methyl orange aqueous solution (10 ppm) by means of ultrasonic waves for 20 min. The suspension was then stirred, and samples were drawn at intervals. The reaction temperature of 27 °C was maintained by a water bath. After stirring at 300 rpm for 30 min in the dark, the adsorption equilibrium was reached, and then, the UV-A or visible light source with an intensity of 1.7 mW/cm^2 was applied and samples were drawn at intervals for analysis of the concentration of methyl orange. A UV–vis spectrometer (Metertech SP-880) was used to determine the concentration of methyl orange by the absorbance of the solution at a wavelength of 465 nm. No detectable degradation of the dyes was observed in the absence of the catalyst or from irradiation with UV and visible light alone. The photocatalytic decolorization reaction followed a pseudo-first order rate law, which was consistent with previous literature [10,22]. The reaction rate law can be expressed as $\ln(1 - X) = -kt$, where k and X are the reaction rate constant and the conversion of methyl orange, respectively.

3. Results and discussion

3.1. Photocatalyst activity under UV and visible-light irradiation

Many researchers use NO oxidation to determine the photocatalytic reactivity in various TiO_2 photocatalytic applications [4,9,19,22,23]. The electron–hole pair (e^-–h^+) generated upon light excitation is trapped at the TiO_2 surface as spatially separated redox active sites. Some studies report the formation of reactive oxygen species, such as superoxide ion ($O_2^{\bullet -}$), atomic oxygen (O), O^-, OH and HO_2 radicals on the surface of TiO_2 irradiated with UV light [2–4]. The general mechanism of NO_x oxidation by a photocatalyst is given below. Hydrogen ions and hydroxide ions are dissociated from water. The active oxygen species are produced on the TiO_2 surface.

$$O_2 + e^- \rightarrow O_2^- \quad (1)$$

$$OH^- + h^+ \rightarrow OH^* \quad (2)$$

$$H^+ + O_2^- \rightarrow HO_2^* \quad (3)$$

Nitric monoxide is oxidized to nitric acid or nitrous acid by active oxygen species. Based on the gas-phase chemistry of NO_x [24], NO is converted to HNO_3 as a consecutive photooxidation via a NO_2 intermediate. Nitric acid is then formed on the catalyst surface.

$$NO + HO_2^* \rightarrow NO_2 + OH^* \quad (4)$$

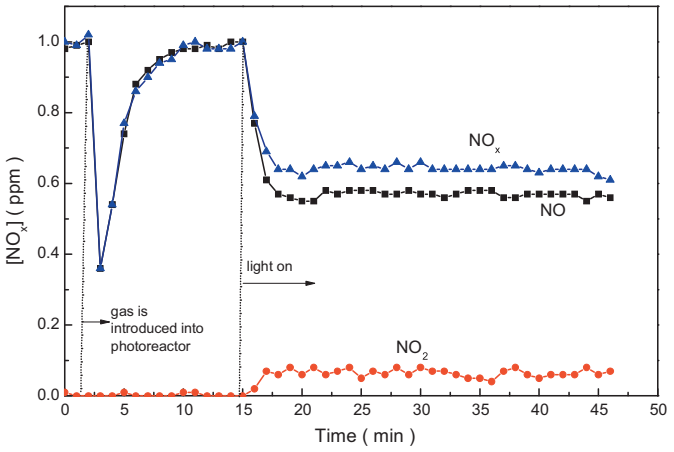

Fig. 1. Time-course of the changes in concentration of NO, NO_2 and NO_x in the presence of TiO2_200 under visible light (blue LED); catalyst loading: 0.2 g, irradiation intensity: 1 mW/cm2, inlet concentration of NO: 1 ppm, inlet flow rate: 1 L/min, reaction temperature: 24 °C, where $[NO]_x = [NO] + [NO_2]$. (For interpretation of the references to color in this figure legend, the reader is referred to the web version of the article.)

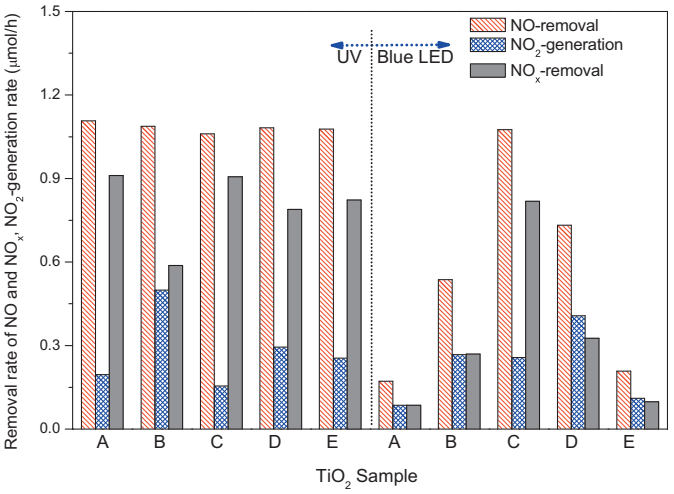

Fig. 2. Average removal rate of NO_x on various photocatalysts under UV and visible-light irradiations; catalyst loading: 0.2 g, irradiation intensity: 1 mW/cm^2, inlet concentration of NO: 1 ppm, inlet flow rate: 1 L/min, reaction temperature: 24 °C.

$$NO_2 + OH^* \rightarrow HNO_3 \quad (5)$$

$$NO + OH^* \rightarrow HNO_2 \quad (6)$$

Photocatalyst activity reduces as acid accumulates. To illustrate the reaction behavior of NO photocatalytic oxidation, 0.2 g of TiO_2_200 and 1 mW/cm^2 of light intensity were used to conduct the experiment. Initially, a 1 ppm NO gas stream was introduced into the photo-reactor under light exclusion. As shown in Fig. 1, the NO concentration in the gas phase dropped owing to NO adsorption onto the TiO_2. After 4–5 min, the NO was saturated on the TiO_2, and the NO gas phase concentration returned to 1 ppm. The steady state of this photocatalytic reaction was achieved as soon as the photocatalyst was illuminated. The NO concentration decreased from 1 to 0.56 ppm, and the NO_2 concentration increased to 0.07 ppm. The NO_x concentration, which includes both NO and NO_2, was maintained at 0.63 ppm for 30 min under blue LED illumination. The activities of these TiO_2 catalysts do not obviously decrease during 30 min of operation, owing to their large surface area (>150 m^2/g).

Fig. 2 shows the NO_x removal and NO_2 generation rates obtained using various photocatalysts under UV and visible-light irradiation. The comparison above used pristine photocatalysts (Ishihara ST01). Under UV illumination, these photocatalysts exhibit a similar activity in NO_x mineralization, with the exception of TiO_2_100 owing to its large NO_2-selectivity (45.9%) ($Sel._{NO2} = [NO_2]_{generated}/[NO]_{converted}$). This indicates that the carbon content of TiO_2_100 is either so high as to reduce the active area of TiO_2 or its carbonaceous structure has a poor affinity to NO_2. Under visible light (blue LED), the activity levels of these photocatalysts were in the order of TiO_2_200 > TiO_2_250 > TiO_2_100 > ST01 ~ TiO_2_300. Therefore, the optimum calcination temperature is 200 °C in this impregnation process, with the visible-light-responsive carbonaceous structure formed most efficiently at 200 °C. The rate of NO_x removal increases as the illumination wavelength decreases; by contrast, the selectivity of NO_2 is increased by increasing the wavelength of the illumination. When comparing the reaction behavior over TiO_2_200 under illumination by UV and blue LED, no significant difference in NO conversion was observed, and the NO_2 concentration was higher under blue LED than under UV light. There are three reasons for the increase in NO_2-selectivity under visible-light irradiation. First, the number of active sites on the TiO_2 surface decreases with an increase in the wavelength of illumination. Second, the visible-light-responsive active site on the TiO_2 potentially exhibits poor oxidative ability or less affinity for NO_2 [9,23]. Third, NO_2 is less readily oxidized than NO [24]. The decreasing reaction rate under visible light for TiO_2_200 is primarily caused by a decrease in the NO_2 oxidation rate.

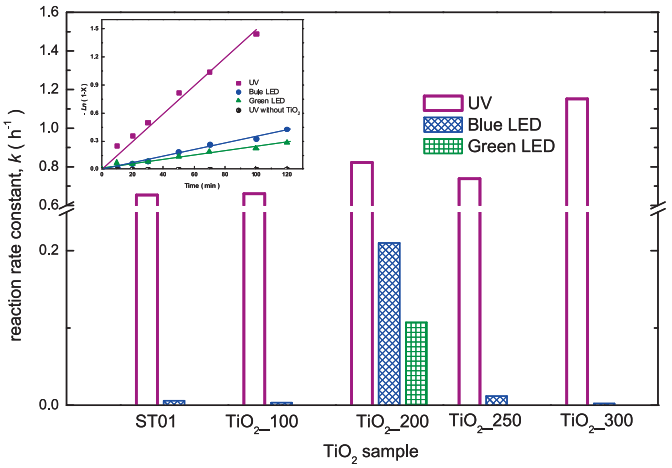

Fig. 3. (a) Decolorization curves of MO over TiO2_200 under various illuminations. (b) Decolorization rate constants of various photocatalysts under UV and visible-light irradiations; catalyst loading: 0.2 g, irradiation intensity: 1.7 mW/cm^2, reaction volume: 200 mL, concentration of MO: 10 ppm, reaction temperature: 27 °C.

Fig. 3(a) shows that the decolorization of dye reaction with TiO_2 is a first-order reaction, with the slope of the straight line giving the rate constant (k) of the degradation of methyl orange. It is well known that some dyes can sensitize titania, such as methylene blue [25,26]. However, these photosensitive materials are not suitable as probe chemicals for photocatalytic activity tests, especially those for the evaluation of activity under visible light. Our results showed that MO is not degraded over pristine TiO_2 (ST01) under visible-light illumination, indicating that MO will not sensitize TiO_2 and is thus a suitable compound to evaluate the visible-light-responsive activity of TiO_2. Summarized rate constants for both UV and visible-light illumination are depicted in Fig. 3(b). The strongest methyl orange decolorization effect was observed with TiO_2_300 under UV illumination (1.15 h^{-1}), and only TiO_2_200 exhibited obvious visible-light-responsive activity (0.21 h^{-1}). Under UV light, the activity levels of these photocatalysts were in the order of TiO_2_300 > TiO_2_200 > TiO_2_250 > TiO_2_100 ~ ST01. When compar-

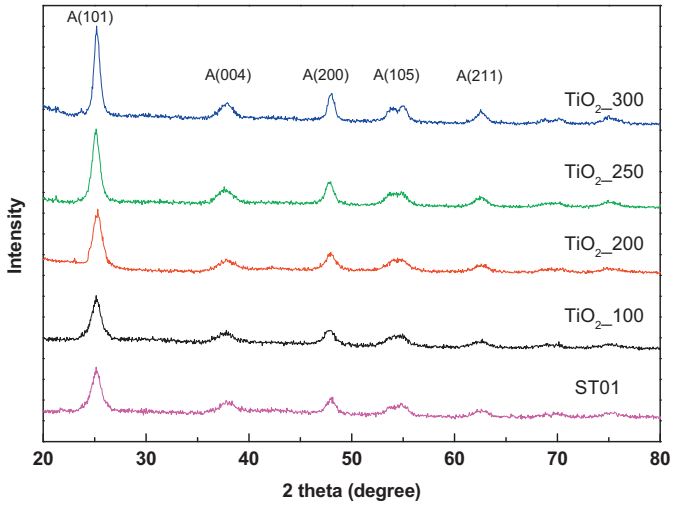

Fig. 4. XRD patterns of prepared photocatalysts.

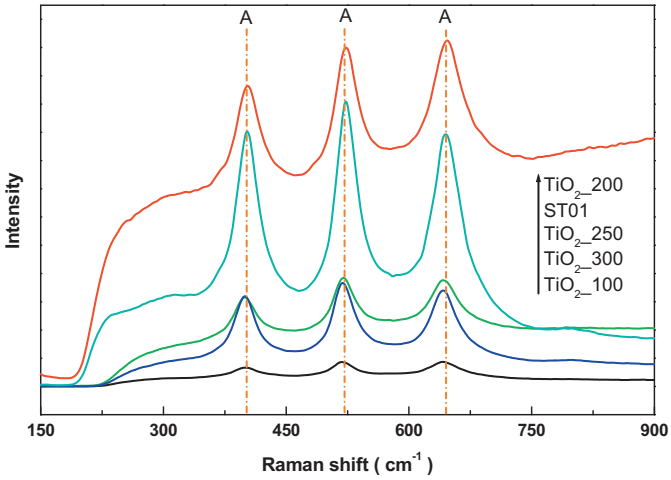

Fig. 5. Raman spectra of prepared photocatalysts.

ing the UV-induced activity levels of these samples in gaseous and aqueous reactions, the presence of carbon only obviously improves the decolorization ability of TiO_2, probably due to its affinity to dye. Furthermore, under visible-light illumination, samples TiO_2_100 and TiO_2_250 performed modestly in the oxidation of NO; however, they showed no activity in the decolorization reaction. Therefore, the influences of carbonaceous structure upon gaseous and aqueous reactions are at least partially different, especially for visible-light-responsive activities.

3.2. TiO_2 photocatalyst characterization

3.2.1. XRD

Fig. 4 shows the X-ray diffraction patterns of TiO_2 samples. The peaks for the (1 0 1), (0 0 4), (2 0 0), (1 0 5), and (2 1 1) reflections characteristic of the TiO_2 anatase phase appeared on all samples. The rutile phase does not appear due to the low-temperature calcination. The crystallite sizes of the prepared photocatalysts are determined from a half width of (1 0 1) peak using the Scherrer formula ($d = 0.9\lambda/\beta\cos\theta$). As shown in Fig. 4, the crystallite size of TiO_2 to gradually increase as the temperature increased. TiO_2_300 shows the largest crystallite size and the highest degree of crystallization. Toyota et al. have suggested that the existence of carbonaceous species retards the growth of TiO_2 crystallite during the heating step [27]. However, in our work, the influence of heating on crystallite growth size is not as obvious as on the degree of TiO_2 crystallization, as shown in Table 1.

3.2.2. Raman spectroscopy

Raman spectroscopy can be used to clearly characterize the TiO_2 surface structure [9,10,28,29]. Raman spectroscopy wave vector selection rules, which limit the wave vector of detectable photons to the Brillouin zone center, break down at a very small size (>10 nm). As a result, all the spectra peaks broadened as the particle size decreased. Iida et al. [28] and Li et al. [29] both claim that this method is more sensitive than X-ray diffraction for nanometer-sized crystals. Our investigations used lower laser power to avoid laser heating or laser damage. Fig. 5 shows TiO_2 Raman spectra at different heating temperatures. The anatase phase, Raman shift = 396, 517, and 638 cm^{-1} [10], existed in all TiO_2 samples. The Raman intensity levels of these photocatalysts were in the order of ST01 > TiO_2_200 ≫ TiO_2_300 > TiO_2_250 > TiO_2_100. The results of the Raman spectra were not consistent with the XRD patterns. Theoretically, the Raman intensity should increase with greater degrees of crystallization. Hence, it shows that the coverage effect of a carbonaceous species on TiO_2 surface results in the decrease of Raman intensity [19]. The coverage ratio should decrease as the temperature increases owing to a reduction in the carbon content through heating, which is evidenced in XPS results (see Table 1). This inference can be used to interpret these Raman spectra with the exception of TiO_2_200. The strong Raman intensity of TiO_2_200 can be explained by two factors. First, the strong Raman scattering of TiO_2_200 is probably attributed to its superior visible-light absorption, as shown in Fig. 7 The Raman scatter intensity of a sample is proportional to its absorption of visible laser (Ar-ion laser) illumination for Raman analysis. Second, the resonance Raman phenomenon [30] is likely caused by the small bandgap of TiO_2_200, leading to a Raman intensity much larger than the well-crystallized TiO_2_300, this good crystallization being evidenced in XRD analysis. Furthermore, the crystal carbon structure, for example the D- and G-bands of graphite at 1350 and 1580 cm^{-1} [31], was not observed in this case, suggesting that the carbonaceous species on the prepared TiO_2 surface is of an amorphous structure [10].

3.2.3. XPS

A number of studies have discussed carbon-doped and carbon-covered titania materials [4,9–21], with researchers reporting that carbonaceous species play the role of sensitizer, inducing visible-light absorption and response. The calcination temperature-dependent property change of the prepared TiO_2 was investigated by XPS analysis. The deconvolution of C 1s XPS spectra for the best visible-light-responsive TiO_2_200 is shown as a representative example in Fig. 6(a). Three XPS peaks occurred at 284.9, 286.4, and 288.9 eV for the prepared TiO_2. The first peak arises from adventitious elemental carbon (C–C), and the other two peaks indicate the existence of C-O, COR(H), and C═O, corresponding to a carbonate spices [9–14,19]. The BE at 284.9 eV that is also observed with the reference ST01 can be ascribed to ambient organic impurities adsorbed on the origin TiO_2 surface, and thus provides little information about the carbon dopants. The BE peaks centered at 286.4 and 288.9 eV are similar to the oxidized carbon species from alcohol [32]. This resulted in the carbonaceous species, existing in a condensed and coke-like structure, remaining on the photocatalyst surface. Another possible assignment of these two peaks is that the carbonate species exists in the form of an interstitial dopant [33]. However, the creation of interstitial carbon dopants during photocatalyst preparation has a large energetic demand, so the low heating temperature (200 °C) used in this process should preclude this possibility. The BE at 281 eV for Ti–C structure is also

Table 1
Selectivity of NO_2, carbon content, crystallite size, and bandgap of TiO_2 samples.

Sample	Sel.$_{NO2}$ under UV (%)	Sel.$_{NO2}$ under VIS (%)	C content (at.%)	Crystallite size[a] (nm)	Bandgap[b] (eV)
TiO_2_100	45.9	49.8	24.5	9.08	3.15
TiO_2_200	14.5	23.9	18.3	9.42	2.83
TiO_2_250	27.1	55.5	16.5	10.28	3.09
TiO_2_300	23.6	52.9	13.8	10.58	3.22
ST01	17.7	50.0	5.63	9.02	3.22

[a] Calculated by Scherrer formula $d = 0.9\lambda/\beta\cos\theta$.
[b] Estimate by UV–vis absorption spectra (Fig. 8).

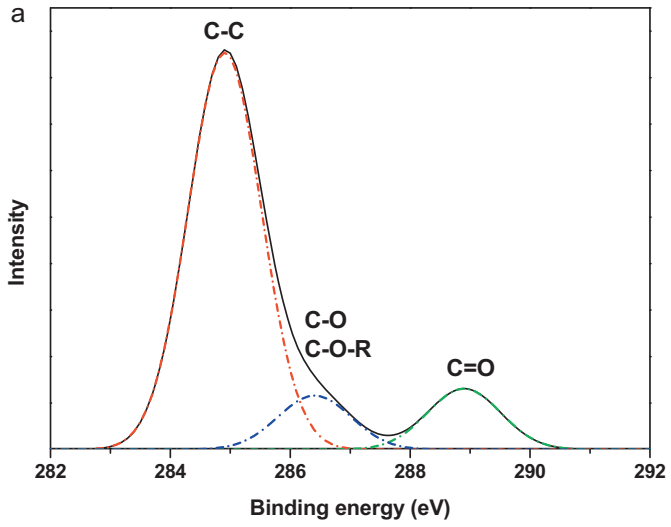

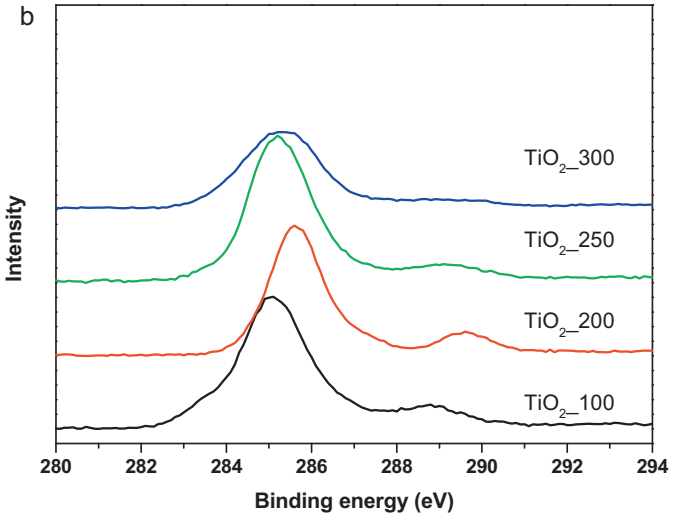

Fig. 6. (a) The deconvolution of C 1s XPS spectra for TiO2_200 and (b) C 1s XPS spectra all carbon-containing samples.

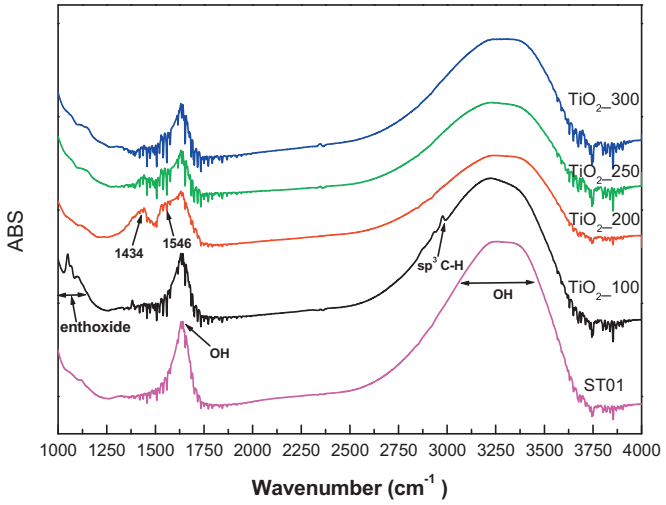

Fig. 7. FTIR spectra of prepared photocatalysts.

not observed due to this mild calcination conditions. The carbonate species on the TiO_2 surface is able to absorb visible light as a photosensitizer [11,12,17,32], and the alcohol on TiO_2 surface will convert to the visible-light-responsive structures at about 200 °C according to the results of photoactivity.

As shown in Fig. 6(b), the intensities associated with the carbonate species (BE peaks at 286.4 and 288.9 eV) increase markedly from TiO_2_100 to TiO_2_200 and then decreased with increasing temperature from 200 to 300 °C. However, the total carbon contents of these TiO_2 samples decreased with increasing temperature from 100 to 300 °C owing to the thermal decomposition of carbonaceous species (see Table 1). The binding energies of the O 1s and Ti 2p orbitals do not vary between the samples, and it depicts the carbon atom does not incorporate into the oxide lattice. The visible-light-responsive activity results from the BE peaks at 286.4 and 288.9 eV, according to the results of XPS and photocatalytic activites. Moreover, following the Ar^+ ion etching process of TiO_2_200, the peak intensities associated with the carbonaceous species decreased; after 60 s of etching, the carbonate species could not be observed on the TiO_2. This shows that the carbonaceous species exists predominantly on the surface, which agrees with our previously reported results in which carbon-containing TiO_2 samples were synthesized in the sol–gel and chemical vapor deposition methods [9,10,19], and this process being much easier than former methods.

3.2.4. *Infrared diffuse reflectance spectra*

Diffuse reflectance infrared Fourier transform spectra (DRIFT) were applied to further investigate the carbonaceous species on the prepared TiO_2 materials, as shown in Fig. 7. The IR data of ST01 show two peaks at 1630 and 3700–2800 cm^{-1}. The first peak corresponds to the OH group on the surface and the second broad peaks is due to the adsorbed water molecules [34]. The intensity of this second peak decreased with increased temperature as adsorbed water was removed via calcination. The TiO_2 surface is covered by carbonaceous species and the adsorbed water is evaporated on heating, so the intensity of the OH peak reasonably becomes smaller after carbon-modification. In a comparison with ST01, the peaks of ethoxide (1020–1120 cm^{-1}) and the sp^3 C–H stretch (2976 cm^{-1}) corresponding to alcohol-impregnation [35] are observed in TiO_2_100. The ethoxide is chemisorbed on TiO_2 surface via mild calcination [35]. Following calcination at 200 °C, the associated peaks disappear and two peculiarly broad peaks at 1434 and 1546 cm^{-1} (the latter being connected with OH peak), appear in the 1200–1800 cm^{-1} region for TiO_2_200. The intensities of these two peaks decrease sharply after calcinations at temperature above 250 °C. These broad peaks can be attributed to combinations of

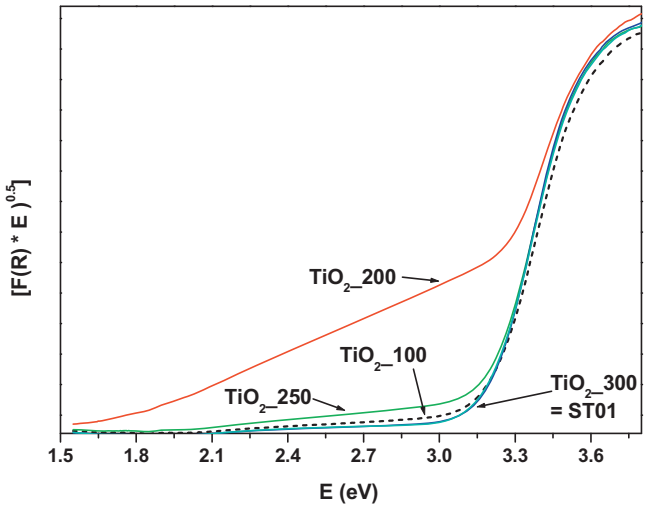

Fig. 8. UV–vis absorption spectra of various photocatalysts.

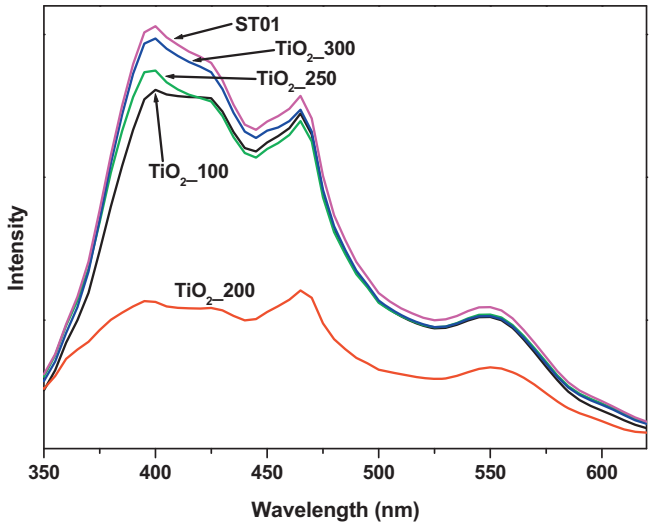

Fig. 9. Photoluminescence spectra of all samples.

O═C–OR, C–H, C═C, and C–O functional groups [34,35]. These functional groups can be roughly ascribed to acetate-like compound [35]. The broad peaks at 1434 and 1546 cm^{-1} correlate to the BE peaks at 286.4 and 288.9 eV in the XPS results. The IR results are consistent with XPS analyses and indicate that the visible-light-sensitized carbonate species is generated during calcination at 200 °C and decomposes at temperature over 250 °C. The residual carbon species on TiO_2_300 are likely to be more highly oxidized structures, for example, alkenes and aromatic rings.

3.2.5. *UV–vis diffuse reflectance spectra*

Fig. 8 shows the UV–vis diffuse reflectance spectra of the prepared TiO_2 materials and ST01. This reflectance data was converted by the instrument software to absorbance values, $F(R)$, based on the Kubelka–Munk theory [11,12,23]. The visible-light absorbance of the prepared TiO_2 samples depended on the synthesis temperature. The visible-light absorption of these photocatalysts was in the order of TiO_2_200 ≫ TiO_2_250 > TiO_2_100 > TiO_2_300 ~ ST01. The spectra showed satisfactory evidence for good activity of TiO_2_200 under visible-light illumination. It is also consistent with the obtained XPS and IR spectral data. In this study, only TiO_2_200 exhibited a good visible-light absorption tail up to over 800 nm, as depicted in Fig. 8. In the TiO_2_200 sample, a sharp edge extended to ~438 nm corresponding to a band gap of ~2.83 eV was observed. However, the observed absorption tails only appeared in the powder calcined at 200 °C and can not be explained its visible-light-responsive activity with the simple band gap shift or narrowing due to this carbon-modification. The degradation of NO and decolorization of dye over TiO_2_200 can still occur under illumination with a green LED peaked at 515 nm (~2.41 eV). Therefore, the carbonate species in the sample may play two roles; it may act as an impurity of TiO_2 to form interface states that effectively lower the band gap, and it may act as a sensitizer for visible-light absorption [9,12–15].

3.2.6. *Photoluminescence spectroscopy*

The rate of recombination of e^-/h^+ pairs may also be a key factor affecting the photoactivity of titania [36,37]. Some species on a TiO_2 surface, for example, metal and anionic atoms, can conduct electrons at room temperature with only small resistance [5,6,36]. Similarly, some carbonaceous species bound to TiO_2 can also conduct electrons easily, with the electrons generated from the TiO_2 by irradiation. Accordingly, the efficiency of recombination of e^-/h^+ pairs in the carbon-containing titania may decrease [38]. Photoluminescence emission spectra were obtained for various photocatalysts, as shown in Fig. 9, to elucidate the fate of e^-/h^+ pairs in semiconductor particles (TiO_2). As anticipated, the pristine TiO_2 photocatalyst (ST01) shows a broad PL emission band, which is similar to that reported in the literature [37]. The ST01 and carbon-containing TiO_2 samples exhibit a similar excitonic PL emission band, indicating that the carbonaceous species does not cause this new PL phenomena. Jing et al. report that the excitonic PL intensity of TiO_2 decreases as the particle size increases, which is ascribed to the decrease in the content of surface oxygen vacancy and defect with increasing particle size [22,37]. The TiO_2 size effect on PL intensity should be not significant here owing to the small difference in grain size between these samples (see Fig. 4). According to the results of XPS and PL, the peak intensity of the PL spectrum increases with a decrease in the carbon content in TiO_2, except for TiO_2_200. The peak intensities of PL spectra of all carbon-containing catalysts are lower than that of pristine TiO_2, indicating that the electron–hole recombination rate of self-trapped excitations in TiO_2 is reduced by the introduction of carbonaceous species [38]. TiO_2_200 exhibits the smallest PL intensity, probably due to its peculiar carbonate structure, evidenced in the characterizations by XPS and IR. Therefore, the effect of the carbonaceous species' structure on reducing the probabil-

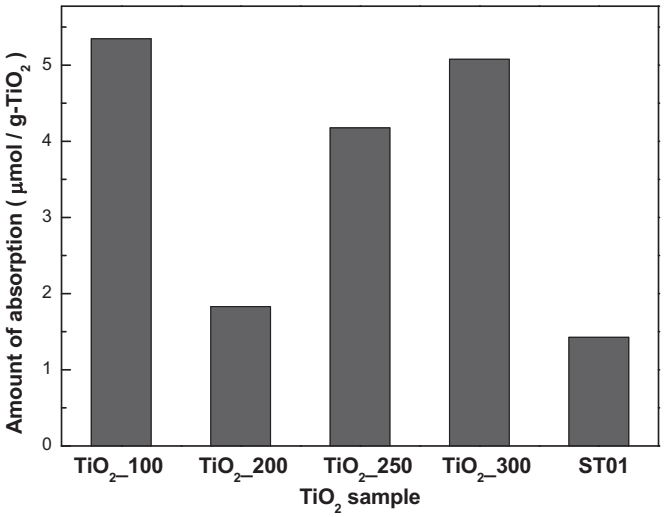

Fig. 10. Dye-adsorbability of all samples: catalyst loading; 0.2 g, reaction volume: 200 mL, concentration of MO: 10 ppm, reaction temperature: 27 °C.

ity of e^-/h^+ recombination is more important than the carbon content. For the above reasons, the results indicate that TiO_2-200 should exhibit the highest photocatalytic activity under both UV and visible irradiations. However, the decolorization rate under UV illumination over TiO_2-200 is less than that over TiO_2-300, revealing that another factors influences its decolorization rate. Accordingly, the adsorbabilities of the dye for the photocatalysts were examined, as shown in Fig. 10. The dye-adsorbability of these photocatalysts is in the order of TiO_2-100 > TiO_2-300 > TiO_2-250 > TiO_2-200 > ST01. The functional groups showing peaks at 1434 cm^{-1} in IR spectra exhibited the worse affinity for methyl orange, so consequently the decolorization rate over TiO_2-200 was not improved as could be anticipated from the PL spectral data. The coverage of TiO_2-100 with carbonaceous species is probably too excessive to reduce its UV-responsive activity even through its adsorbability is reasonable. The better decolorization activity for TiO_2-300 can be attributed to the superior crystallization [37] and its good affinity for the dye.

4. Conclusions

Carbon-containing TiO_2 photocatalysts were successfully prepared by an impregnation process using ethanol as the carbon source. Carbon-containing TiO_2 (TiO_2-200) shows a relatively high photocatalytic activity for NO_x oxidation and dye decolorization under visible-light illumination. The optimal synthesis temperature is 200 °C to covert alcohols to a carbonate structure, as evidenced by XPS, IR, and UV–vis absorption spectra. It is responsible for the observed good visible-light absorption and photo-activity. The visible-light activity and absorption of prepared TiO_2 is sharply decreased by calcination at temperatures higher than 250 °C. This carbonate structure (BE peaks at 286.4 and 288.9 eV; IR absorption regions at 1434 and 1546 cm^{-1}) is also able to reduce the probability of e^-/h^+ recombination, but does not have a good affinity to the methyl orange. In conclusion, this simple and energy-efficient process for the production of visible-light-responsive photocatalysts can be applied to purify water and air, both in indoor and outdoor environments.

Acknowledgements

The authors wish to acknowledge our two anonymous reviewers for their excellent comments. The authors would like to thank the National Science Council for financial support under the grant no. NSC-97-2218-E-011-005.

References

[1] A. Fujishima, K. Honda, Nature 238 (1972) 37.
[2] M.R. Hoffmann, S.T. Martin, W. Choi, D.W. Bahnemann, Chem. Rev. 95 (1995) 69.
[3] A. Fujishima, N.R. Tata, A.T. Donald, J. Photochem. Photobiol. C 1 (2000) 1.
[4] Y.M. Lin, Y.H. Tseng, J.H. Huang, C.C. Chao, C.C. Chen, I. Wang, Environ. Sci. Technol. 40 (2006) 1616.
[5] E. Kowalska, R. Abe, B. Ohtani, Chem. Commun. (2009) 241.
[6] M.R. Elahifard, S. Rahimnejad, S. Haghighi, M.R. Gholami, J. Am. Chem. Soc. 129 (2007) 9552.
[7] I. Nakamura, N. Negishi, S. Kutsuna, T. Ihara, S. Sugihara, K. Takeuchi, J. Mol. Catal. A 161 (2000) 205.
[8] R. Asahi, T. Morikawa, T. Ohwaki, K. Aoki, Y. Taga, Science 293 (2001) 269.
[9] Y.H. Tseng, C.S. Kuo, C.H. Huang, Y.Y. Li, P.W. Chou, C.L. Cheng, M.S. Wong, Nanotechnology 17 (2006) 2490.
[10] S.Y. Treschev, P.W. Chou, Y.H. Tseng, J.B. Wang, E.V. Perevedentseva, C.L. Cheng, Appl. Catal. B 79 (2008) 8.
[11] S. Sakthivel, H. Kisch, Angew. Chem. Int. Ed. 42 (2003) 4908.
[12] C. Lettmann, K. Hildenbrand, H. Kisch, W. Macyk, W.F. Maier, Appl. Catal. B 32 (2001) 215.
[13] P. Zabek, J. Eberl, H. Kisch, Photochem. Photobiol. Sci. 8 (2009) 264.
[14] E.A. Konstantinova, A.I. Kokorin, S. Sakthivel, H. Kisch, K. Lips, Chimia 61 (2007) 810.
[15] J. Orth-Gerber, H. Kisch, U.S. Pat. US 2005226761 (2005) (Kronos International Inc., Germany).
[16] S. Yin, M. Komatsu, Q. Zhang, F. Saito, T. Sato, J. Mater. Sci. 42 (2007) 2399.
[17] T. Ohno, M. Akiyoshi, T. Umebayashi, K. Asai, T. Mitsui, M. Matsumura, Catal. Lett. 98 (2004) 255.
[18] S.U.M. Khan, M. Al-Shahry, W.B.I. Jr., Science 297 (2002) 2243.
[19] C.S. Kuo, Y.H. Tseng, C.H. Huang, Y.Y. Li, J. Mol. Catal. A 270 (2007) 93.
[20] H. Irie, Y. Watanabe, K. Hashimoto, Chem. Lett. 32 (2003) 772.
[21] S.W. Hsu, T.S. Yang, T.K. Chen, M.S. Wong, Thin Solid Films 515 (2007) 3521.
[22] Y.C. Hsiao, Y.H. Tseng, Micro Nano Lett. 5 (2010) 317.
[23] T. Sano, N. Negishi, K. Koike, K. Takeuchi, S. Matsuzawa, J. Mater. Chem. 14 (2004) 380.
[24] R. Atkinson, D.L. Baulch, R.A. Cox, R.F. Hampson Jr., J.A. Kerr, J. Troe, J. Phys. Chem. Ref. Data 18 (1989) 881.
[25] X. Yan, T. Ohno, K. Nishijima, R. Abe, B. Ohtani, Chem. Phys. Lett. 429 (2006) 606.
[26] B. Ohtani, Chem. Lett. 7 (2008) 216.
[27] M. Toyoda, Y. Yoshikawa, T. Tsumura, M. Inagaki, J. Photochem. Photobiol. A 171 (2005) 167.
[28] Y. Iida, M. Furukawa, T. Aoki, T. Sakai, Appl. Spectrosc. 52 (1998) 673.
[29] M. Li, Z. Feng, G. Xiong, P. Ying, Q. Xin, C. Li, J. Phys. Chem. B 105 (2001) 8107.
[30] S.A. Asher, Anal. Chem. 65 (1993) 59A.
[31] E. Terrado, M. Redrado, E. Muñoz, W.K. Maser, A.M. Benito, M.T. Martínez, Diamond Relat. Mater. 15 (2006) 1059.
[32] M. Janus, B. Tryba, M. Inagaki, A.W. Morawaski, Appl. Catal. B 52 (2004) 61.
[33] R. Fu, N. Yoshizawa, M.S. Dresselhaus, G. Dresselhaus, J.H. Satcher Jr., T.F. Baumann, Langmuir 18 (2002) 10100.
[34] Y. Huang, W. Ho, S. Lee, L. Zhang, G. Li, J.C. Yu, Langmuir 24 (2008) 3510.
[35] I.C. Kang, Q. Zhang, S. Yin, T. Sato, F. Saito, Appl. Catal. B 80 (2008) 81.
[36] Y. Yu, J.C. Yu, C.Y. Chan, Y.K. Che, J.C. Zhao, L. Ding, W.K. Ge, P.K. Wong, Appl. Catal. B 61 (2005) 1.
[37] L. Jing, Y. Qu, B. Wang, S. Li, B. Jiang, L. Yang, W. Fu, H. Fu, J. Sun, Sol. Energy Mater. Sol. Cell 90 (2006) 1773.
[38] C. Yu, J.C. Yu, Catal. Lett. 129 (2009) 462.